Experimental and DFT studies on structure, spectroscopic and thermal properties of N-Methyl-N,N,N-trioctylammonium chloride ionic liquid

Mohammed Amin Assenine, Boumediene Haddad, Annalisa Paolone, Silvia Antonia Brandán, Didier Villemin, Mostefa Boumediene, Mustapha Rahmouni, Serge Bresson

Experimental and DFT studies on Structure, spectroscopic and thermal properties of N-Methyl-N,N,N-trioctylammonium chloride ionic liquid

Mohammed Amin Assenine [1], Boumediene Haddad [2,3,4], Annalisa Paolone [5] , Silvia Antonia Brandán[6,*] Didier Villemin [3], Mostefa Boumediene [2], Mustapha Rahmouni [4], Serge Bresson[7].

[1] Université Djillali Liabes, BP 89, 22000 Sidi-Bel-Abbes, Algeria

[2] Chemistry Laboratory of Synthesis, Properties, and Applications (CLSPA-Saida), 20000 Saida, Algeria.

[3] LCMT, ENSICAEN, UMR 6507 CNRS, University of Caen, 6 bd Ml Juin, 14050 Caen, France

[4] Synthesis and Catalysis Laboratory LSCT, Tiaret University, Tiaret, Algeria

[5] CNR-ISC, U.O.S. La Sapienza, Piazzale A. Moro 5, 00185 Roma, Italy

[6] Cátedra de Química General, Instituto de Química Inorgánica, Facultad de Bioquímica. Química y Farmacia, Universidad Nacional de Tucumán, Ayacucho 471, (4000) San Miguel de Tucumán, Tucumán, Argentina.

[7] Laboratoire de Physique des Systèmes Complexes, Université Picardie Jules Verne, 33 rue St Leu 80039 Amiens cedex, France.

*Corresponding author: Tel.: +54-381-4247752; fax: +54-381-4248169;

E- mail: silvia.brandan@fbqf.unt.edu.ar (S.A. Brandán).

ABSTRACT

The [Aliquat$^+$][Cl$^-$] ionic liquid (IL) has been structural and vibrationally characterized combining experimental FT-IR, FT-Raman and ^{1}H- and ^{13}C-NMR spectroscopies with theoretical studies based on the hybrid B3LYP/6-31G* method. The theoretical determination of structure of IL in gas phase and aqueous solution by using that level of theory shows three ionic C-H···Cl bonds, as supported by atomic Merz-Kollman (MK) charges, bond orders, natural bond orbital (NBO) and atoms in molecules (AIM) calculations. Hence, a monodentate coordination between the [Aliquat$^+$] cation and Cl anion has been proposed for IL because only one of three ionic C-H···Cl bonds presents higher energy and lower distance. The optimized structure confirmed by NMR measurements has allowed the assignments of 237 normal vibration modes to the bands observed in the infrared and Raman spectra with the aid of scaled quantum mechanical force field (SQMFF) methodology and the normal internal coordinates. The effect of Cl in the IL is the shifting of vibration modes corresponding to the CH_2 and CH_3 groups, as compared with the cation. The mapped MEP surface evidence a strong concentration of charges around the chloride anion compatible with nucleophilic sites

in these regions while the frontier orbital analyses suggest that IL is most reactive than the cation probably due to the low values of both global electrophilicity and nucleophilicity indexes. The thermal stability shows that [Aliquat$^+$][Cl$^-$] start to decompose just above 200°C. Comparisons between [Aliquat$^+$][Cl$^-$] and [Aliquat$^+$][NTf$_2^-$] ILs show that the IL containing chloride is most reactive than the other one while [Aliquat$^+$] [NTf$_2^-$] is thermally more stable than [Aliquat$^+$][Cl$^-$]. These results suggest that the properties of an IL containing the [Aliquat$^+$] cation are strongly dependent of anion. In addition, the scaled force constants for the [Aliquat$^+$][Cl$^-$] IL are also calculated and compared with the reported for the cation. The Cl anion modifies in notable form the properties of cation.

KEYWORDS: Aliquat 336, ionic liquid; FT-IR, FT-Raman; thermal analysis; DFT calculations.

1. INTRODUCTION

The interesting physicochemical properties and applications that present the ionic liquids (ILs) have allowed the gradual growth in the investigations of these species from different points of view [1-14]. For instance, the quaternary ammonium salt, known as Aliquat 336, presents characteristics properties and major applications [15-20]. Besides, the synthesis reactions of these ionic liquids are environmentally benign and friendly due to its stability against air and moisture and; in addition, these salts are easy to handle [16,17,20]. Studies on Aliquat 336 containing chloride anion have suggested that its use is limited by the strong coordination effect of that halogen [17]. Hence, the cation-anion interactions play a very important role in the properties of ILs [4,5,9,12]. Currently, the elucidations of all types of interactions in ILs are carried out combining theoretical calculations with different spectroscopic techniques [9,12,14,15]. So far, various quaternary ammoniums ILs with different cations and anions have been reported for Aliquat 336, including a recent study on the synthesis and structural and thermal properties of [Aliquat$^+$][NTF$_2^-$] IL [15-31] but the structural, electronic, vibrational and topological properties of [Aliquat$^+$][Cl$^-$] IL was no reported yet. Hence, the aims of this work are: (i) to optimize the structure of [Aliquat$^+$][Cl$^-$] IL in order to predict structural, electronic, topological and vibrational properties, (ii) to find the coordination mode between cation and anion by using natural bond orbital (NBO) and atoms in molecules (AIM) calculations, (iii) to characterize experimentally [Aliquat$^+$][Cl$^-$] IL by using the infrared, Raman, ^{1}H- and ^{13}C-NMR spectra and, (vi) to perform comparisons of this IL with the reported for [Aliquat$^+$][NTF$_2^-$] IL [15]. In this work, the experimental infrared (FTIR/ATR) and Raman spectra of [Aliquat$^+$][Cl$^-$] IL were recorded and its structure in gas

phase was optimized by using the B3LYP/6-31G* method [32,33]. Then, the structure of it was confirmed by using ^{1}H, ^{13}C and ^{19}F-NMR spectroscopies. The combinations of vibrational spectra with the DFT calculations and the scaled mechanical force field (SQMFF) methodology have allowed the determination of harmonic force field and the scaled force constants [34-36]. The normal internal coordinates for the cation were taken of those proposed for [Aliquat^{+}][NTF_2^{-}] IL [15] while the used transferable scaling factors were those recommended for the method employed by Rauhut and Pulay [35]. The investigations of reactivity and behaviours of [Aliquat^{+}][Cl^{-}] IL were evaluated taking into account the frontier orbitals and some interesting descriptors [9,12,15]. Then, all obtained properties were compared with compounds with similar cations [15] while the complete assignments of 237 vibration modes expected for [Aliquat^{+}][Cl^{-}] IL were reported for first time in the present work.

2. Experimental

2.1. Materials and methods

The chemicals used in this study are N-Methyl-N,N,N-trioctylammonium chloride (> 99%) and lithium bis (trifluoromethylsulfonyl) Imide (99%). They were purchased from Aldrich and used as received. Deionized H_2O was obtained with a Millipore ion-exchange resin deionizer. The structures of the ionic liquids prepared and studied in the present work are shown in **Scheme 1**.

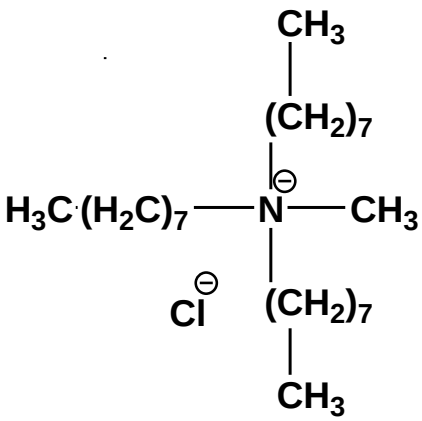

Scheme 1: Structure of investigated IL [Aliquat^{+}][Cl^{-}].

2.2. General procedure for the synthesis of Aliquat 336 ILs

Firstly, the quaternary ammonium salt ([Aliquat$^+$][Cl$^-$]) is obtained commercially and was used as received. Before use ([Aliquat$^+$][Cl$^-$]) was dried in phosphorus pentoxide, P_2O_5, to remove residual water. The water content was below 300 ppm; this measure was carried out by coulometric Karl Fischer titration performed by means of a Metrohm 831.

2.3. NMR analysis

The structure of investigated IL ([Aliquat$^+$][Cl$^-$]) was checked by NMR in order to probe the desired structure and confirm their purity. ^{1}H-NMR (400 MHz) and ^{13}C NMR (100.6 MHz) spectra were recorded on a DRX 400 MHz spectrometer (400 MHz). The chemical shifts (δ) are given in ppm and referred to the internal solvent signal namely tetramethylsilane (TMS) and $CDCl_3$.

2.4. Thermal analysis

Concomitant measurements of thermogravimetry (TGA) and differential thermal analysis (DTA) were performed by means of a Setaram Setsys Evolution 1200 TG System, with a fixed temperature rate of 5°C/min, in an argon flux of 60 ml/min. For each sample, an initial mass of ~20 mg was used.

2.5. Vibrational spectroscopy

2.5.1. FTIR/ATR measurements

The FTIR/ATR measurements were acquired on a Bruker Vertex II-70RAM Spectrometer (Bruker Analytical, Madison, WI) operating with a Golden Gate diamond ATR accessory TM (Specac Ltd, Slough, United Kingdom). The FTIR/ATR spectra were collected with 1 cm^{-1} nominal resolution by co-adding 64 scans for each spectrum in the range 600-4000 cm^{-1}. The OPUS Software 6.0 for Windows was used for the management of the instrument.

2.5.2. FT-RAMAN measurements

FT-RAMAN spectra were acquired on a Vertex 70-RAM II Bruker FT-Raman spectrometer. This instrument is equipped with a Nd:YAG laser (yttrium aluminium garnet crystal doped with triply ionized neodymium) with a wavelength of 1064 nm and a maximum power of 1.5 W. The measurement accessory is pre-aligned: only the Z-axis of the scattered light is adjusted to set the sample in the appropriate position regarding the local measurement point. The RAM II spectrometer is equipped with a liquid nitrogen cooled Ge detector. FT-Raman

spectra were collected with 1 cm^{-1} resolution by co-adding 128 scans for each spectrum at room temperature in the range 45-4000cm^{-1}. The OPUS 6.0 software was used for the spectral acquisition, manipulation and transformation. These both measurements FTIR/ATR and FT-RAMAN were performed in the Walloon Agricultural Research Center (Craw) Belgium.

3. Computational details

The modelled of [Aliquat$^+$][Cl$^-$] was carried out with the *GaussView* program [37] while its optimization in gas phase was performed by using the functional hybrid B3LYP/6-31G* level of theory with the Revision A.02 of Gaussian 09 program [32,33,38]. The determination of properties of [Aliquat$^+$][Cl$^-$] in gas phase were evaluated by using the natural bond orbital (NBO), the Bader's theory of atoms in molecules (AIM) 2000 programs [39-41] and atomic charges derived from semiempirical methods [42]. The frontier orbitals were used to obtain the energy gap values while with these parameters were computed the chemical potential (μ), electronegativity (χ), global hardness (η), global softness (S), global electrophilicity index (ω) and global nucleophilicity index (E) descriptors [9,12,15]. After that, the complete vibrational assignments of [Aliquat$^+$][Cl$^-$] was performed by using the scaled mechanical force field (SQMFF) procedure with the normal internal coordinates of cation taken of Ref [15] for [Aliquat$^+$][NTf_2^-] IL and with the Molvib program [34-36]. Potential energy distribution (PED) contributions ≥ 10 % and transferable scaling factors were employed to perform the vibrational assignments of IL [35]. To a better correlation the Raman spectra predicted in activities were corrected to intensities by using typical equations [43,44]. Finally, the ultraviolet-Visible and ^{1}H and ^{13}C NMR spectra were predicted by using Time-dependent DFT calculations (TD-DFT) together and the GIAO method at the same level of theory [45]. The volume calculations of cation and IL were computed the Moldraw program [46]. The calculations in solution were performed by using a methodology similar to other ionic liquids [9,12].

4. Results and discussion

4.1. NMR results

Figure 1 (a and b) shows the NMR spectra versus chemical shift dissolved in ($CDCl_3$) over the scan range 0 to 10 δ ppm for ^{1}H NMR and from 0 to 150 δ ppm for ^{13}C NMR for [Aliquat$^+$][Cl$^-$] IL. ^{1}H and ^{13}C-NMR spectra indicates and confirm the absence of any impurities in our investigated IL.

As shown in Figure 1 (a), the signals at δ =3.14-3.18 ppm in [Aliquat$^+$][Cl$^-$] were assigned to the methylene protons on the alkyl rings N^+–$(CH_2)_n$–. The signal at δ =2.98 ppm corresponding to the N^+-CH_3, thus, another three signals in the range of δ =1.64, broad at δ =1.25-1.33 ppm andδ =0.85-088 ppm were attributed to the methylene N^+–(CH_2)—(CH_2)– and –$(CH_2)_n$– groups in octyl chains and terminal methyl group –$(CH_2)_n$—CH_3respectively.

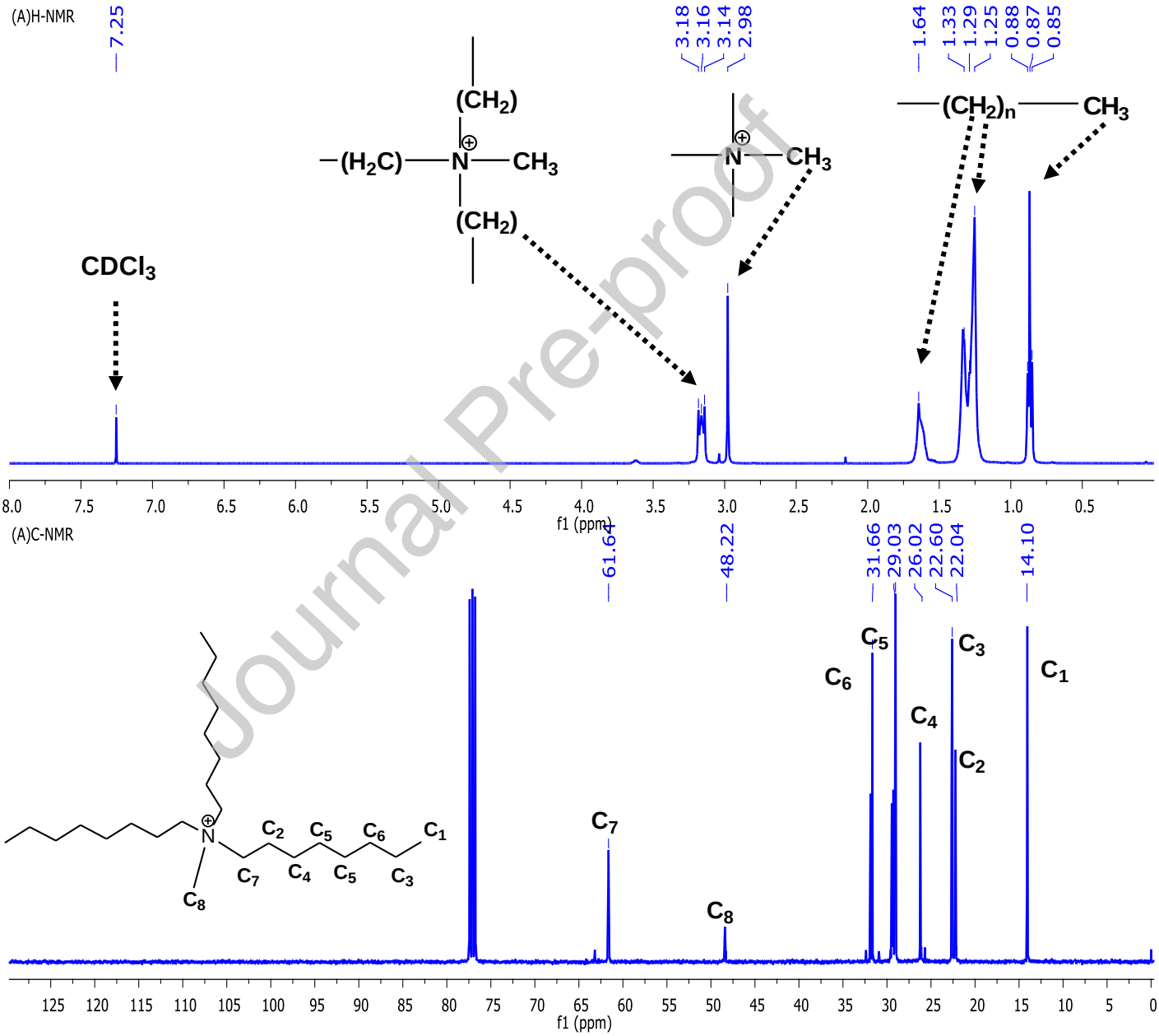

Figure 1. Hydrogen atom labeling and ^{1}H NMR (a), carbon atom labeling and ^{13}C NMR (b) in $CDCl_3$. of ([Aliquat$^+$][Cl$^-$]).

Moreover, the ^{13}C-NMR spectrum of ([Aliquat$^+$][Cl$^-$]) was found to have eight signals over the range δ= 0 –65 ppm confirming the presence of the hydrocarbon skeleton.

The spectroscopic data are given below and the H and C atom labeling and the corresponding spectra are shown in Figure 1 (a and b).

[Aliquat$^+$][Cl$^-$]: ^{1}H-NMR (400 MHz, ($CDCl_3$) δ_H (ppm)= 3.14-3.18 (N^+–$(CH_2)_n$–, 6H), 2.98 (N^+-CH_3,3H), 1.64 (N^+–(CH_2)—(CH_2)–, 6H), 1.25-1.33 (–$(CH_2)_n$–, 30H), 0.85-088 (–$(CH_2)_n$––CH_3, J=4 Hz, 9H).^{13}C-NMR (100.6 MHz, ($CDCl_3$) δ_C (ppm): δ= 61.64 (C7), 48.22 (C8), 31.66 (C6), 29.03 (C5), 26.02(C4), 22.60 (C3), 22.04 (C2), 14.10 (C1).

4.2. Computational results

4.2.1. Geometrical parameters

Optimized structures of [Aliquat$^+$][Cl$^-$] and its cation in gas phase by using the B3LYP/6-31G* method can be seen in **Figure 2** while in **Table 1** are reported the uncorrected and corrected energy values by zero point vibrational energy (ZPVE) for those two species together with the dipole moment values and volumes by using the B3LYP/6-31G* method.

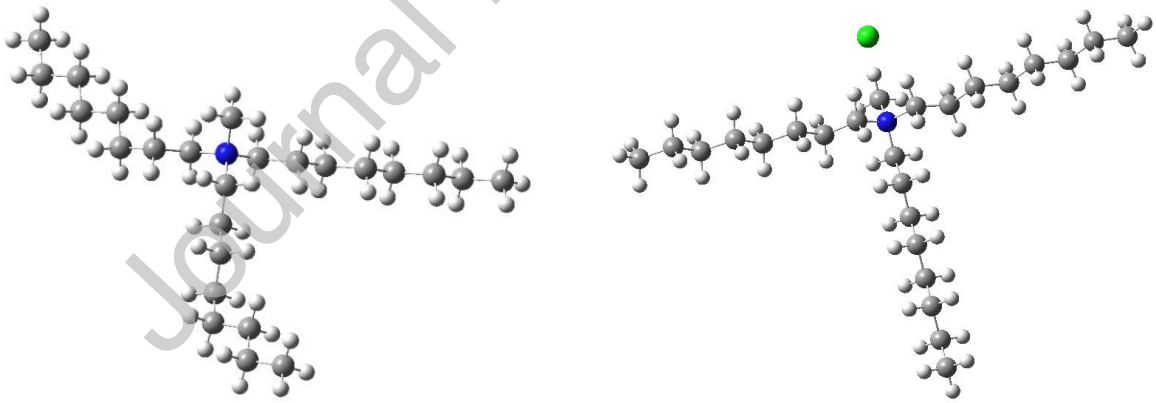

Figure 2. Optimized structures of [Aliquat$^+$][Cl$^-$] and its cation by using the B3LYP/6-31G* method.

Table 1. Calculated uncorrected and corrected total energies (*E*), dipole moments (μ) and volumes (V) of [Aliquat$^+$][Cl$^-$] and its cation in gas phase by using the B3LYP/6-31G* method.

B3LYP/6-31G* Method					
Species	E	ZPVE	μ (D)	V (Å^3)	ΔV
[Aliquat$^+$][Cl$^-$]	-1500.1637	-1499.3967	12.60	533.2	39.3

[Aliquat$^+$]	-1039.7644	-1038.9980	4.67	493.9

The results show that the incorporation of Cl anion to cation generates a higher dipole moment value and a slight increase in the volume, with an expansion in the volume of 39.3 Å^3. However, the position and orientation of dipole moment vector of [Aliquat+][Cl-] ionic liquid in gas phase by using the B3LYP/6-31G* level of theory is different from that observed for the cation, as shown in **Figures 3a** and **3b**. Thus, in the cation the vector is orientated from the N atom in direction to N-CH_3 group while in the IL it is oriented from the N atom but in the opposite direction, as clearly shows the Fig. 3b. Hence, the Cl anion modifies in notable form the properties of cation. Main moieties of [Aliquat$^+$][Cl$^-$] IL and its cation showing the atoms labelling and the N, C, H and Cl atoms involved in cation-anion interactions are shown in **Figure S1** of supporting material. The calculations performed in solution by using the PCM method evidence a compression in the volume and an increase in the dipole moment value (18.8 D).

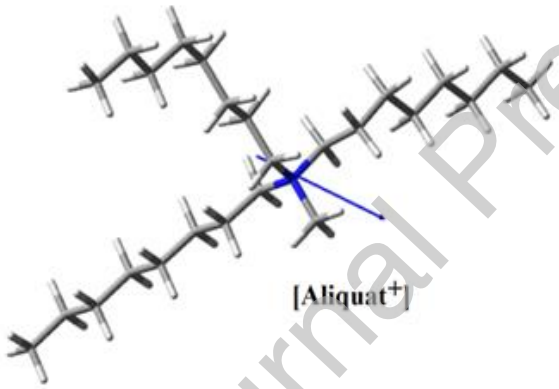

Figure 3a. Orientation and direction of dipole moment vector corresponding to cation of [Aliquat$^+$][Cl$^-$] ionic liquid in gas phase by using the B3LYP/6-31G* level of theory.

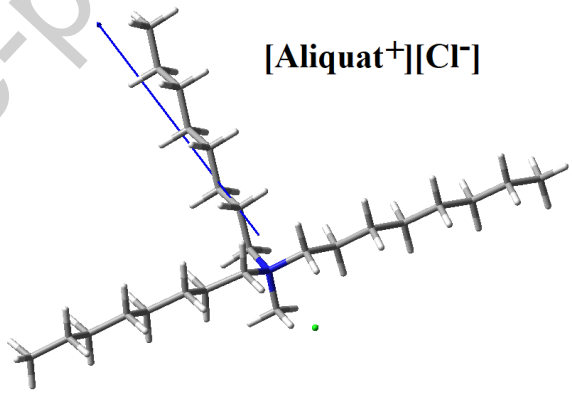

Figure 3b. Orientation and direction of dipole moment vector of [Aliquat$^+$][Cl$^-$] ionic liquid in gas phase by using the B3LYP/6-31G* level of theory.

The values predicted for closest H6-Cl81, H31-Cl81 and H78-Cl81 distances between cation and anion these are distances between the Cl anion and the H atoms of CH_3 (H78) and two next CH_2 groups (H6 and H31) of cation, they are respectively 2.423, 2.380 and 2.404 Å, higher than the value 1.81 Å obtained computationally for the protic analogue of the [Aliquat$^+$] cation [47,48]. The distance between both N1 and Cl81 atoms is 3.661 Å. Obviously, in solution the H6-Cl81, H31-Cl81 and H78-Cl81 distances of interactions increase at 2.783, 2.881 and 2.779 Å, respectively.

4.2.2. Atomic charges, molecular electrostatic potentials (MEP) and bond orders

Cation-anion interactions of [Aliquat$^+$][Cl$^-$] IL were studied in gas phase by using the hybrid B3LYP/6-31G* method and the atomic Mulliken, Merz-Kollman (MK) and NPA charges, molecular electrostatic potentials (MEP) and bond orders (BO), expressed as Wiberg indexes. The results only for the involved atoms in cation-anion interactions of IL, these are the N1, C5, C30, C77, H6, H31, H78 and Cl81 atoms are presented in **Table S1** of supporting material compared with the values corresponding to its cation. Comparisons between the moieties structures of IL and its cation with the numbering of main involved atoms in the cation-anion interactions can be observed in Fig S1 while the behaviours of calculated MK, Mulliken and NPA charges on the N1, C5, C30, C77, H6, H31 and H78 atoms of [Aliquat$^+$][Cl$^-$] IL and its cation in gas phase by using the B3LYP/6-31G* method are given in **Figure S2**. This latter figure shows that the three types of charges on the atoms of both species present practically the same behaviours, however, the MK charges on the [Aliquat$^+$][Cl$^-$] IL shows a significant difference, as compared with the other ones. The MK charge on N1 has a positive sign in cation while the other two charges on this atom present negative signs. Hence, the presence of Cl atom in the IL produces that MK charge on N1 become negative. In the same way, the MK charges on C5 and C30 have positive signs while the other two charges evidence negative values on these atoms of both species. These changes in the signs of charges on the C atoms obviously modify the values and signs of MK charges on the H6, H31 and H78 atoms. Thus, the MK charge on H6 atom has negative sign while on the H31 presents positive sign in the IL. These studies clearly reveal that the MK charges show differences between the IL and its cation due to the presence of Cl and to interactions cation-anion, for these reasons, these atomic MK charges could explain the different properties between both species.

If now the molecular electrostatic potentials (MEP) for the two species are analyzed from Table S1 it is observed that the Cl atom presents the most negative value, as expected, because it atom is the most electronegative atom while the remain ones present the following tendency: Cl > N> C > H. On the other hand, the less negative MEP values are observed on the H atoms. The MEP values between both species are practically the same, however, the mapped MEP surface, shown in **Figure S3**, suggests a highest electron density accumulate around the Cl atom in [Aliquat$^+$][Cl$^-$] IL. Hence, the strong red colour is observed on the most electronegative Cl atom revealing nucleophilic sites on the entire region. Then, slight light blue colours are observed on H atoms of some CH_2 groups of side chain while the other two side chains show green colours characteristics of inert regions.

Other interesting properties analyzed in both species are the bond orders (BO) expressed as Wiberg indexes which can be seen in Table S1. The BO values of N1 in both [Aliquat$^+$][Cl$^-$] IL and its cation practically are constant while change slightly the values for the other atoms. Here, a very important resulted is observed in the BO value for the Cl atom because it is 0.277, which reveals the important coordination modes that it atom present. Thus, when the Wiberg bond index matrix in the NAO basis values are analyzed we observed that the BO values for the H6, H31 and H78 are respectively of 0.0533, 0.0572 and 0.0545 while for the C5, C30 and C77 are respectively of 0.0245, 0.0269 and 0.0270 whose total value is 0.243, a few lower than the total by atom of 0.277. This way, the C5-H6, C30-H31 and C77-H78 bonds are engaged in certain form in cation-anion interactions. These important results evidence three ionic bonds between IL and its cation through the chlorine atom. The graphic with the Moldraw program presented in **Figure 4** shows a tridentate coordination mode of Cl atom to cation in the [Aliquat$^+$][Cl$^-$] IL [46].

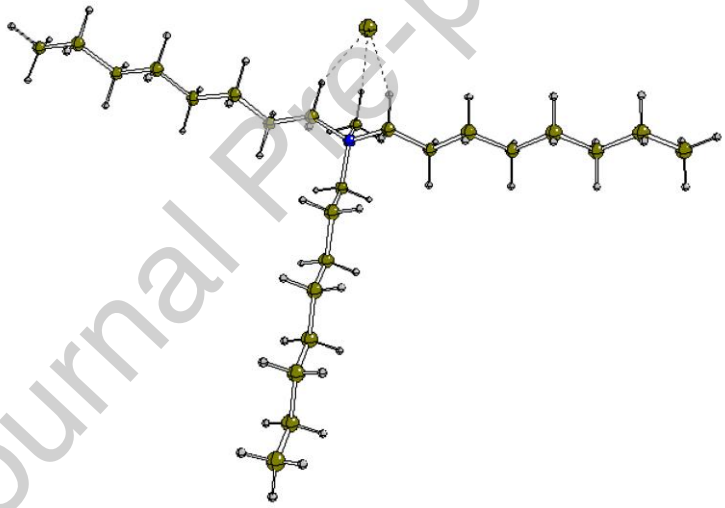

Figure 4. Coordination modes of Cl atoms to cation in the [Aliquat$^+$][Cl$^-$] IL.

4.2.3. NBO and AIM studies

The above studies have evidenced clearly that the Cl atom is tri-coordinate to cation by means of the C2-H46, C11-H47 and C2-H65 bonds, as supported by atomic MK charges and bond orders values of involved atoms. For these reasons, it is necessary to investigate the formation of other intra-molecular or H bonds interactions in addition to those ionic bonds. Hence, the second order perturbation theory analyses of Fock matrix in NBO Basis by using the NBO program and the topological properties with the AIM 2000 program were used in order to

predict if some of those other interactions are observed in the [Aliquat$^+$][Cl$^-$] IL in gas phase by using the B3LYP/6-31G* method [39-41]. Hence, the first analysis performed for the IL by using the NBO program shows only three interactions with higher energy values, which are the *LP(4)Cl81→σ*C5-H6*, *LP(4)Cl81→σ*C30-H31* and *LP(4)Cl81→σ*C77-H78* interactions with values respectively of 23.78, 31.27 and 24.91 kJ/mol with a total energy value of 79.96 kJ/mol. Note that the second interaction is stronger than the other ones because the distance between H31 and Cl81 is 2.308 Å. All these interactions are performed from lone pairs of Cl atom to antibonding sigma C5-H6, C30-H31 and C77-H78 orbitals. Here, it is necessary to clarify that the cation of IL does not show interactions in both media, as was evidenced in the study of [Aliquat$^+$] [NTf_2^-] [15]. These interactions correspond to those ionic predicted previously by MK charges and bond orders, supporting newly the characteristics ionic of these interactions.

The second analysis by AIM program using the topological properties and the Bader's theory of atoms in molecules is useful to investigate the characteristic or nature of intra-molecular, H bonds, ionic and covalent polar interactions [40,41]. Then, the electron density, $\rho(r)$, the Laplacian values, $\nabla^2\rho(r)$, the eigenvalues ($\lambda1$, $\lambda2$, $\lambda3$) of the Hessian matrix and, the $|\lambda1|/\lambda3$ ratio have been calculated in the bond critical points (BCPs) and ring critical points (RCPs) for the [Aliquat$^+$][Cl$^-$] IL in gas phase by using the B3LYP/6-31G* method. In the cation of IL in gas phase are not observed new interactions while in the IL are observed six interactions (BCPs) which origin six RCPs and one cage critical point (CCP). The CCP is formed when several rings form a cage (see point green colour). The new interactions have different characteristics because the C8-H10···H80 and C77-H79···H35 interactions are of H bonds while the other four C5-H6···Cl81, C30-H31···Cl81, C77-H78···Cl81 and C39-H40···Cl81 are ionic interactions and, all of them can be clearly observed in **Figure 5**.

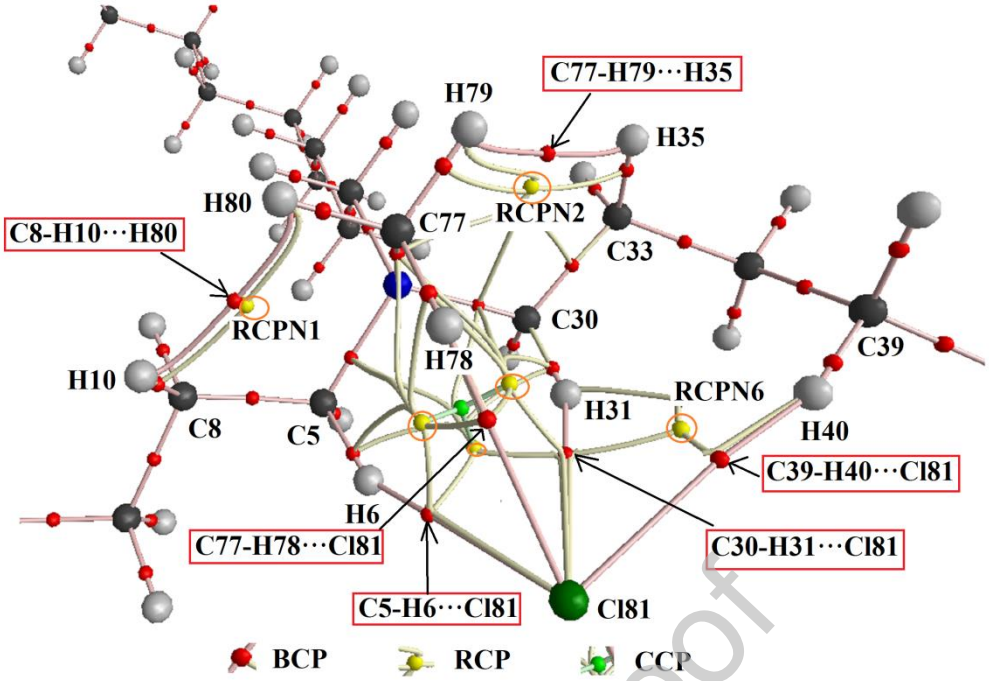

Figure 5. Molecular graphic for the [Aliquat$^+$][Cl$^-$] IL in gas phase showing the geometry of all their bond critical points (BCPs), ring critical points (RCPs) and cage critical point (CCP) by using the B3LYP/6-31G* method.

The ionic or highly polar covalent interactions have $\lambda 1/\lambda 3 < 1$ and $\nabla^2\rho(r) > 0$ (closed-shell interaction) while the eigenvalues of the Hessian matrix in the CCPs have all positive signs. The topological properties of all those new interactions are presented in **Table S2** together with the distances between the two involved atoms in each interaction. RCPN1 and RCPN2 are named to the RCPs of both C8-H10···H80 and C77-H79···H35 interactions (see orange circles on yellow RCP in Fig. 5) while RCPN3, RCPN4 and RCPN5 are named to the RCPs formed between H6 and H31, H6 and H78 and H6 and H31, as can be easily seen from Figure 5. Finally, RCPN6 corresponds to that RCP generates by the C39-H40···Cl81 interaction. Note that the distances between the two atoms involved in both H···H interactions present lower values than the distances of the other ones. In solution, only the C5-H6···Cl81, C30-H31···Cl81, C77-H78···Cl81 and C77-H79···H35 interactions are observed while the other two disappear in this medium. These AIM studies have revealed two H bonds interactions and other ionic one in addition to those three ionic predicted also by NBO analysis.

4.2.4. Frontier orbitals and global descriptors analyses

The predictions of gap values and behaviour of [Aliquat$^+$][Cl$^-$] IL by means of the frontier orbitals, HOMO and LUMO are very important taking into account that the quaternary

ammonium salts present characteristics properties and major applications [15-20]. This way, calculations of HOMO, LUMO, energy band gaps and chemical potential (μ), electronegativity (χ), global hardness (η), global softness (S), global electrophilicity index (ω) and global nucleophilicity index (E) descriptors [9,12,15] are presented in **Table S3** for the [Aliquat$^+$][Cl$^-$] IL by using the B3LYP/6-31G* method together with the values for the cation and the equations used in the calculations of descriptors. These results are compared in the same table with the parameters reported for the [Aliquat$^+$][NTf$_2^-$] ionic liquid in gas phase at the same level of theory [15]. The gap value observed for the cation is 8.2152 eV, a value slightly higher than the observed for the IL (5.7329 eV) and, for this reason, the reactivity of IL increase with the addition of Cl atom to cation. The comparisons between the gap values for [Aliquat$^+$][Cl$^-$] and [Aliquat$^+$][NTf$_2^-$] show that the IL containing chloride is most reactive than the other one. Evidently, the incorporations of Cl$^-$ and [NTf$_2^-$] anions increase the reactivities of both ILs. If now the descriptors are analyzed, it is observed that the two global electrophilicity (ω) and global nucleophilicity (E) indexes have lower values in the [Aliquat$^+$][Cl$^-$] IL than the cation, however, these two indexes for the cation have lower values, as compared with the corresponding to [Aliquat$^+$][NTf$_2^-$] IL. This study shows that the properties of an IL formed by the [Aliquat$^+$] cation are strongly dependent of anion.

4.3. Thermal analysis

The thermal stability of [Aliquat$^+$][Cl$^-$] studied in this work were investigated by means of concomitant TGA/DTA measurements (see Figure 6). This IL is thermally stable up to ≈210 °C. The corresponding DTA signal shows an endothermic peak, attributed and confirm to the thermal decomposition.

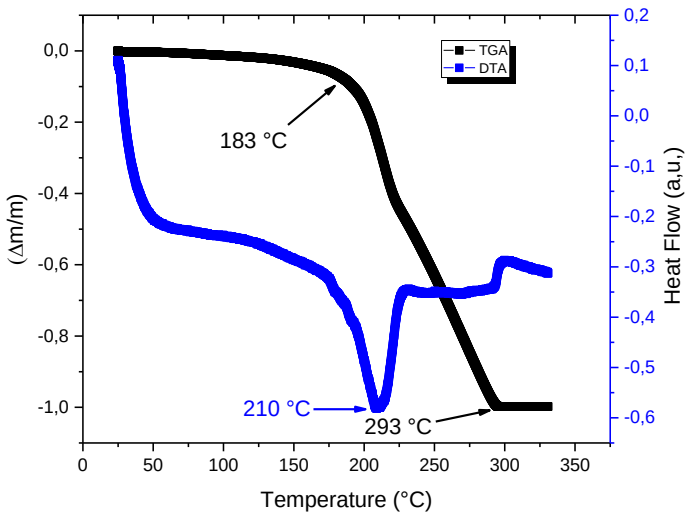

Figure 6: TGA and DTA curves of ([Aliquat$^+$][Cl$^-$]) IL.

Differently from Mikkola el al [17], it seems that decomposition of this IL occurs at a higher temperature compared to the same cation [Aliquat$^+$] with [BH_4^-], T_d : 144 °C; [SO_2^-] , T_d :157 °C; [CH_3COO^-], T_d :175 °C, [$H_2PO_4^-$], T_d : 176, [HSO_4^-] T_d : 196, [$HCOO^-$]; T_d : 174 °C, and with [HCO_3^-] anion, T_d :176 °C and at a lower temperature compared to ([Aliquat$^+$][PF_6^-]) ; T_d : 274 °C, and ([Aliquat$^+$][NTf_2^-]) ; T_d : 367/383 °C [15, 17]. Indeed, this difference is strongly depends on the type of anion and due to related cation–anion interaction type.

4.4. Vibrational study

Many works have evidenced that the FTIR/ATR and Raman spectroscopies are techniques perfectly suited for the analysis of ionic liquids [9,12,14,15]; hence, the vibrational measurements of [Aliquat$^+$][Cl$^-$] IL have been carried out using FTIR-ATR and Raman spectra. Comparisons of experimental ATR and Raman spectra of [Aliquat$^+$] [Cl$^-$] IL in solid phase with the corresponding predicted for the IL and its cation in gas phase by using the hybrid B3LYP method can be seen in **Figures 7** and **8**, respectively. The [Aliquat+][Cl$^-$] IL in the gas phase was optimized with C_1 symmetry by using B3LYP/6-31G* calculations and, due to the 81 atoms present in its structure, 237 vibration modes are expected in this IL. All these expected vibration modes present activity in both infrared and Raman spectra. The vibrational analysis and the assignments for the [Aliquat$^+$] cation with their 234 vibration modes were reported in a previous work on the [Aliquat+][NTf_2^-] IL and, for this reason, here the assignments performed for [Aliquat+][Cl$^-$] IL were compared with that available previously for [Aliquat$^+$] from Ref [15]. The determination of harmonic force field of IL was performed with the scaled quantum mechanical force field (SQMFF) procedure taking into account the normal internal coordinates of cation, transferable scaling factors and the Molvib program [15,34-36]. Here, the quaternary N atom of IL was considered with C_{3V} symmetry, as in the definition of normal internal coordinates of cation [15] while a monodentate coordination between cation and anion was proposed for IL because the only interaction with higher energy and lower distance is the C30-H31⋯Cl81 interaction. In **Table 2** are summarized observed and calculated wavenumbers and assignments for the [Aliquat$^+$][Cl$^-$] IL and its cation in gas phase by using the hybrid B3LYP Method. Then, assignments for the most important groups are discussed below.

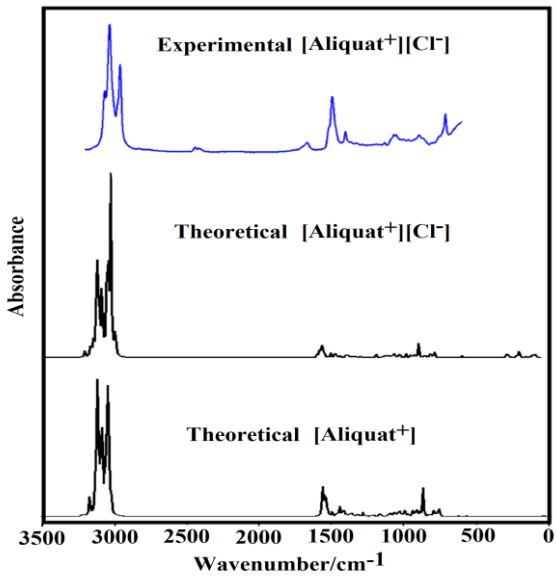

Figure 7. Experimental Infrared spectra of [Aliquat$^+$] [Cl$^-$] IL in solid phase compared with the predicted for the cation and IL in gas phase by using the hybrid B3LYP method.

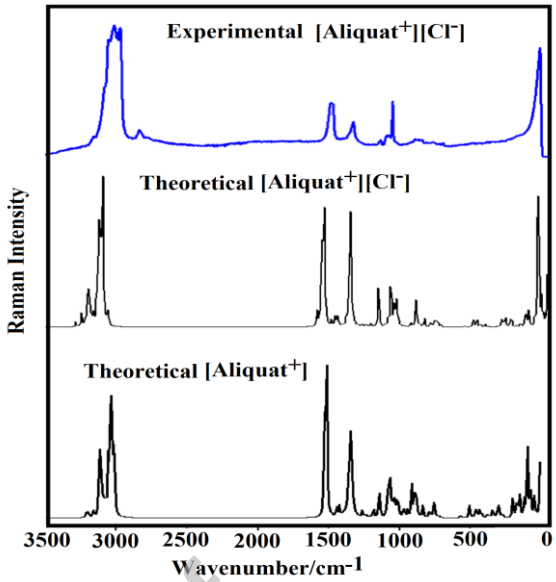

Figure 8. Experimental Raman spectra of [Aliquat$^+$] [Cl$^-$] IL in solid phase compared with the predicted for the cation and IL in gas phase by using the hybrid B3LYP method.

4.4.1. Bands assignments

4.4.1.1. 4000-2000 cm^{-1} region. In this region, the anti-symmetric and symmetric stretching modes of CH_2 and CH_3 groups are expected for [Aliquat$^+$] [Cl$^-$] IL and its cation. In both species there are four terminal CH_3 groups (C26, C51, C73, C77) where three of them belong to larges side chains (C26, C51, C73) while the remains belong to N-CH_3 group (C77). The two anti-symmetric modes of N-CH_3 group of IL are predict by SQM calculations between 3060 and 3026 cm^{-1} while the symmetric one at 2875 cm^{-1}, hence, these modes are assigned to the shoulders observed in Raman at 3067 and 2880 cm^{-1}, respectively. Note that the anti-symmetric stretching modes of remain CH_3 groups of both species are predicted combined with anti-symmetric modes of CH_2 groups. In Table 2 are presented the descriptions of these modes together with their corresponding assignments based on the SQM calculations.

Table 2. Observed and calculated wavenumbers (cm^{-1}) and assignments for [Aliquat$^+$][Cl$^-$] ionic liquid and its cation in gas phase by using the hybrid B3LYP Method.

Experimental[a]		B3LYP/6-31G* Method			
		[Aliquat$^+$][b]		[Aliquat$^+$][Cl$^-$]	
IR	Raman	SQM[c]	Assignments[b]	SQM[c]	Assignments[a]
		3081	$\nu_a CH_3$(C77)	3060	$\nu_a CH_3$(C77)
	3067sh	3068	$\nu_a CH_3$(C77)	3026	$\nu_a CH_3$(C77)
		3032	$\nu_a CH_2$(C30)	3016	$\nu_a CH_2$(C2)
	3029sh	3030	$\nu_a CH_2$(C2)	3002	$\nu_a CH_2$(C5)

3004m	3019sh	3023	ν_aCH_2(C5)	2994	ν_aCH_2(C30)
	2995sh	2993	ν_aCH_3(C51)	2985	ν_aCH_3(C73)
2992sh		2992	ν_aCH_3(C26)	2983	ν_aCH_3(C26)
		2992	ν_aCH_3(C73)	2981	ν_aCH_3(C51)
2986sh	2987sh	2987	ν_sCH_2(C2)	2978	ν_aCH_3(C26)
2983sh		2984	ν_sCH_3(C77)	2978	ν_aCH_3(C73)
		2982	ν_aCH_3(C51)	2977	ν_aCH_3(C51)
		2982	ν_aCH_3(C26)	2974	ν_aCH_2(C55)
		2980	ν_aCH_3(C73)	2973	ν_sCH_2(C2)
		2980	ν_sCH_2(C30)	2969	ν_aCH_2(C8)
2977sh		2976	ν_aCH_2(C55)	2958	ν_aCH_2(C39)
		2975	ν_aCH_2(C8)	2954	ν_aCH_2(C33)
2971vs	2970s	2973	ν_aCH_2(C33)	2953	ν_aCH_2(C11)
2965sh		2967	ν_sCH_2(C5)	2949	ν_aCH_2(C67),ν_aCH_2(C64)
		2962	ν_aCH_2(C36)	2948	ν_aCH_2(C58)
2956sh		2953	ν_aCH_2(C58)	2945	ν_aCH_2(C45)
		2953	ν_aCH_2(C17)	2944	ν_aCH_2(C17)
		2952	ν_aCH_2(C64)	2933	ν_sCH_2(C55)
2947sh		2949	ν_aCH_2(C42)	2931	ν_aCH_2(C23)
		2942	ν_aCH_2(C11)	2930	ν_aCH_2(C70)
		2936	ν_aCH_2(C70)	2930	ν_aCH_2(C36)
		2935	ν_aCH_2(C48)	2927	ν_aCH_2(C61)
		2933	ν_sCH_2(C55)	2920	ν_aCH_2(C48)
		2932	ν_sCH_2(C8)	2918	ν_sCH_3(C73)
		2932	ν_sCH_2(C33)	2917	ν_aCH_2(C14)
		2931	ν_aCH_2(C23)	2916	ν_aCH_2(C42)
2924sh	2928vs	2930	ν_aCH_2(C61)	2916	ν_sCH_3(C26)
		2920	ν_aCH_2(C14)	2916	ν_sCH_3(C73), ν_aCH_2(C67)
		2920	ν_sCH_3(C26)	2915	ν_sCH_3(C51)
		2920	ν_sCH_3(C51)	2913	ν_sCH_2(C33)
		2919	ν_sCH_2(C36)	2911	ν_sCH_2(C8)
		2919	ν_sCH_3(C73)	2911	ν_aCH_2(C20)
2915sh		2916	ν_aCH_2(C67)	2905	ν_sCH_2(C70)
		2914	ν_aCH_2(C45)	2904	ν_sCH_2(C23)
		2913	ν_aCH_2(C20)	2904	ν_sCH_2(C58)
2912sh		2910	ν_aCH_2(C39)	2901	ν_sCH_2(C36)
		2909	ν_sCH_2(C11)	2901	ν_sCH_2(C11)
		2909	ν_sCH_2(C58)	2897	ν_sCH_2(C61)
		2908	ν_sCH_2(C70)	2897	ν_sCH_2(C48)
		2907	ν_sCH_2(C48)	2897	ν_sCH_2(C30), ν_sCH_2(C30)
2903s		2904	ν_sCH_2(C23)	2896	ν_sCH_2(C64)
		2901	ν_sCH_2(C64)	2895	ν_sCH_2(C17)
		2900	ν_sCH_2(C42)	2891	ν_sCH_2(C45)
		2898	ν_sCH_2(C61)	2890	ν_sCH_2(C67)
		2898	ν_sCH_2(C14)	2889	ν_sCH_2(C14)
2894sh	2893vs	2893	ν_sCH_2(C17)	2886	ν_sCH_2(C20)
		2890	ν_sCH_2(C67)	2886	ν_sCH_2(C39)
2890sh		2890	ν_sCH_2(C45)	2881	ν_sCH_2(C42)
2887sh	2880sh	2890	ν_sCH_2(C20)	2875	ν_sCH_3(C77), ν_sCH_2(C30)

2887sh	2880sh	2886	ν_sCH_2(C39)	2868	ν_sCH_2(C5)
1547sh	1507sh	1496	δCH_2(C42), δC39C42C45	1508	δC30H31Cl81
1526m	1497sh	1486	δ_aCH_3(C77)	1483	δ_aCH_3(C77)
	1476m	1476	δCH_2(C17), δCH_2(C14)	1478	δCH_2(C30)
		1475	δCH_2(C55),δCH_2(C58)	1477	δ_aCH_3(C26)
		1474	δ_aCH_3(C73)	1476	δCH_2(C39),δ_aCH_3(C51)
		1473	δ_aCH_3(C26)	1474	δCH_2(C55)
		1472	δ_aCH_3(C51)	1474	δ_aCH_3(C73)
		1465	δ_aCH_3(C51)	1472	δ_aCH_3(C51), δCH_2(C39)
		1465	δ_aCH_3(C73)	1471	δCH_2(C30)
		1465	δCH_2(C30), δCH_2(C2)	1468	δ_aCH_3(C77), δCH_2(C2)
		1464	δCH_2(C8)	1465	δCH_2(C8)δCH_2(C17)
		1464	δ_aCH_3(C26)	1464	δ_aCH_3(C73), $\rho'CH_3$(C73)
		1462	δCH_2(C36), δCH_2(C39)	1464	δ_aCH_3(C51)
		1462	δCH_2(C64)	1464	δ_aCH_3(C26)
		1461	δ_aCH_3(C77)	1463	δCH_2(C67), δCH_2(C64)
		1459	δCH_2(C39), δCH_2(C58)	1462	δCH_2(C33)
	1455sh	1457	δCH_2(C33)	1461	δCH_2(C33), δCH_2(C45)
		1457	δCH_2(C45)	1458	δCH_2(C5)
		1454	δCH_2(C2)	1457	δCH_2(C8), δCH_2(C55)
1452sh		1453	δCH_2(C55), δCH_2(C8)	1453	δCH_2(C36)
		1450	δCH_2(C70), δCH_2(C48)	1453	δCH_2(C23)
		1450	δCH_2(C48)	1451	δCH_2(C70)
		1450	δCH_2(C70), δCH_2(C23)	1450	δCH_2(C11)
1448sh	1448sh	1447	δCH_2(C17),δCH_2(C14)	1449	δCH_2(C42)
		1447	δCH_2(C67)	1449	δCH_2(C48)
		1446	δCH_2(C36), δCH_2(C39)	1447	δCH_2(C67), δCH_2(C64)
		1446	δCH_2(C61)	1447	δCH_2(C20)
1443w		1446	δCH_2(C20), δCH_2(C11)	1447	δCH_2(C14)
		1441	δCH_2(C5),δCH_2(C30)	1447	δCH_2(C45)
		1432	$wagCH_2$(C30)	1446	δCH_2(C61), δCH_2(C58)
		1423	ρCH_2(C2)	1423	ρCH_2(C2)
1407vw		1407	$wagCH_2$(C45)	1420	$wagCH_2$(C39)
		1406	$wagCH_2$(C67)	1415	$wagCH_2$(C30),$wagCH_2$(C5)
		1404	$wagCH_2$(C39), $wagCH_2$(C42)	1407	$wagCH_2$(C67),$wagCH_2$(C61)
		1402	$wagCH_2$(C58), $wagCH_2$(C61)	1405	$wagCH_2$(C11)
	1399vw	1401	$wagCH_2$(C20), $wagCH_2$(C11)	1404	$wagCH_2$(C58)
		1395	$wagCH_2$(C14)	1404	$wagCH_2$(C45) $wagCH_2$(C48)
		1394	δ_sCH_3(C77)	1402	δ_sCH_3(C77)
		1388	$wagCH_2$(C5)	1396	$wagCH_2$(C20) $wagCH_2$(C23)
		1385	δ_sCH_3(C73)	1384	δ_sCH_3(C73)
		1383	δ_sCH_3(C51)	1382	δ_sCH_3(C26)
		1381	δ_sCH_3(C26)	1381	δ_sCH_3(C51)
		1372	$wagCH_2$(C36)	1379	ρCH_2(C5)
1368w		1371	$wagCH_2$(C64), $wagCH_2$(C70)	1370	$wagCH_2$(C64)
	1365sh	1365	$wagCH_2$(C14),$wagCH_2$(C5)	1370	$wagCH_2$(C14), $wagCH_2$(C8)
		1362	$wagCH_2$(C55)	1366	$wagCH_2$(C36), $wagCH_2$(C42)
		1359	ρCH_2(C5), ρCH_2(C30)	1360	$wagCH_2$(C61),$wagCH_2$(C55)
	1347sh	1344	$wagCH_2$(C33), ρCH_2(C36)	1348	$wagCH_2$(C33)

	1333w	1336	wagCH_2(C23)	1339	wagCH_2(C23)
		1329	wagCH_2(C2), ρCH_2(C55)	1336	wagCH_2(C2), wagCH_2(C23)
1326vw		1328	wagCH_2(C48)	1331	wagCH_2(C2), ρCH_2(C55)
	1320sh	1324	ρCH_2(C58), ρCH_2(C61)	1325	ρCH_2(C58),ρCH_2(C61)
	1316sh	1316	ρCH_2(C39), ρCH_2(C48)	1320	ρCH_2(C39)
	1316sh	1316	ρCH_2(C67)	1318	ρCH_2(C11)
	1316sh	1315	ρCH_2(C11)	1317	ρCH_2(C30)
		1314	ρCH_2(C45), ρCH_2(C42)	1313	ρCH_2(C67)
	1309sh	1310	ρCH_2(C23),ρCH_2(C8)	1312	ρCH_2(C45), ρCH_2(C42)
		1307	ρCH_2(C70),ρCH_2(C64)	1308	ρCH_2(C23),ρCH_2(C20)
		1304	ρCH_2(C23), ρCH_2(C30)	1306	ρCH_2(C70),ρCH_2(C64)
	1291sh	1297	wagCH_2(C67),wagCH_2(C55)	1295	wagCH_2(C67)
		1292	ρCH_2(C48), ρCH_2(C36)	1293	ρCH_2(C48)
		1285	wagCH_2(C8)	1289	wagCH_2(C8)
		1280	ρCH_2(C14)	1281	ρCH_2(C14), ρCH_2(C8)
		1272	ρCH_2(C70)	1271	ρCH_2(C70)
		1265	ρCH_2(C30)	1269	wagCH_2(C42),wagCH_2(C45)
		1263	wagCH_2(C58)	1264	wagCH_2(C64),wagCH_2(C55)
		1247	ρCH_2(C36), wagCH_2(C42)	1250	ρCH_2(C36)
1237vw	1232sh	1237	ρCH_2(C20)	1238	ρCH_2(C20), ρCH_2(C23)
		1230	wagCH_2(C14)	1231	wagCH_2(C14)
		1226	ρCH_2(C33)	1222	ρCH_2(C33)
		1220	ρCH_2(C64), ρCH_2(C67)	1220	ρCH_2(C64), ρCH_2(C67)
		1188	ρ'CH_3(C77)	1195	ρCH_3(C77)
1183vw		1181	ρCH_2(C14)	1185	ρCH_3(C77)
		1168	ρCH_2(C39)	1174	ρCH_2(C14), ρCH_2(C11)
	1156sh	1164	ρCH_3(C77)	1166	ρCH_2(C36)
1141sh	1145w	1143	ρ'CH_3(C77)	1150	ρ'CH_3(C77)
		1128	ρCH_3(C51)	1128	ρCH_3(C26)
1126w		1126	ρCH_3(C51)	1123	ρCH_3(C51)
1108w		1109	ρCH_3(C73)	1109	ρCH_3(C73)
1102sh	1100w	1101	ρCH_3(C73)	1101	$\delta_s NC_3$
1096sh		1096	τwCH_2(C36)	1095	νC30-C33
	1072sh	1083	ρ'CH_3(C26)	1080	ρ'CH_3(C26)
1069sh	1068m	1063	νC2-C55	1068	τwCH_2(C30)
	1055sh	1059	νC5-C8	1064	νC5-C8
		1050	νC61-C64,νC64-C67	1050	νC61-C64,νC64-C67
	1041sh	1042	νC36-C39,νC39-C42	1040	τwCH_2(C5)
		1039	νC45-C48,νC42-C45	1038	νC36-C39νC33-C36
		1037	νC58-C61	1038	νC45-C48νC42-C45
		1034	νC17-C20	1034	νC17-C20,νC20-C23
1028w		1029	δC33C36C39	1032	νC48-C51
		1026	νC11-C14,νC14-C17	1029	νC11-C14,νC14-C17
	1023sh	1025	νC67-C70	1026	νC67-C70
		1013	νC30-C33	1017	νC39-C42,νC30-C33
		1013	νC70-C73	1015	νC55-C58,νC2-C55
		1008	νC55-C58	1013	νC70-C73
		1005	νC8-C11,νC23-C26	1009	νC8-C11
		1000	νC55-C58	1005	νC55-C58,νC48-C51

	985sh	988	νC5-C8	992	νC11-C14,νC5-C8
983sh		981	νC58-C61	983	νC58-C61
		977	ν_aNC_3	981	ν_aNC_3
		970	νC17-C20	971	νC17-C20,νC23-C26
959w		958	νN1-C77	952	ν_aNC_3
935sh		933	νC61-C64	949	νN1-C77
		926	ν_aNC_3	934	νC61-C64
917sh	912w	920	νC33-C36, ρ'CH_3(C51)	926	ρ'CH_3(C51)
		893	ρCH_3(C73) νC67-C70	898	τwCH_2(C30)
		885	ρCH_3(C51)	891	ρCH_3(C73), νC67-C70
881sh		881	ρCH_3(C26), νC20-C23	878	ρCH_3(C26)
	877sh	872	ρCH_3(C51)	875	τwCH_2(C5)
861sh		865	ρ'CH_3(C73)	868	νC45-C48,τwCH_2(C30)
		858	τwCH_2(C20)	861	τwCH_2(C20)
	839vw	844	ν_aNC_3	850	ν_aNC_3
		835	τwCH_2(C20), τwCH_2(C14)	838	τwCH_2(C20)
828sh		825	τwCH_2(C36)	828	τwCH_2(C45),τwCH_2(C36)
804sh	797vw	801	ν_aNC_3	801	ν_aNC_3
789m	752vw	758	ν_sNC_3	766	ν_sNC_3
	731vw	732	τwCH_2(C64)	738	τwCH_2(C14)
729sh	731vw	730	τwCH_2(C30),τwCH_2(C36)	732	τwCH_2(C64)
		725	τwCH_2(C5)	728	τwCH_2(C36)
		706	τwCH_2(C2), τwCH_2(C61)	712	τwCH_2(C30), τwCH_2(C33)
696w		702	τwCH_2(C33),τwCH_2(C30)	707	τwCH_2(C2)τwCH_2(C61)
		686	τwCH_2(C23), τwCH_2(C20)	687	τwCH_2(C23)
		675	τwCH_2(C58),τwCH_2(C55)	676	τwCH_2(C39), τwCH_2(C48)
		671	τwCH_2(C48)	675	τwCH_2(C11), τwCH_2(C8)
		669	τwCH_2(C11), τwCH_2(C8)	672	τwCH_2(C58),τwCH_2(C55)
	665vw	663	τwCH_2(C67) ,τwCH_2(C70)	663	τwCH_2(C45), τwCH_2(C42)
		660	τwCH_2(C42),τwCH_2(C39)	662	τwCH_2(C67), τwCH_2(C70)
	574vw	585	δC8C5N1, δN1C30C33	585	δC8C5N1,δN1C30C33
	529vw	533	δN1C2C55, δC58C61C64	536	δN1C2C55
		509	δ_aNC_3	508	ρNC3,δaNC3,δC5C8C11
	484vw	499	δC36C39C42	500	δC8C11C14, δC11C14C17 δC17C20C23
		475	δC36C39C42	472	δ_sNC_3
		460	δ_sNC_3	463	δ_sNC_3 ,δC20C23C26
	431vw	433	δC33C36C39, δC45C48C51	432	δC14C17C20
		428	δC2C55C58	428	τC11-C14
		416	τC11-C14	422	δC39C42C45 δC45C48C51,δC33C36C39
		396	δC67C70C73,δC61C64C67	398	δC67C70C73, δC61C64C67
	375vw	373	δC30C33C36	376	δC30C33C36
		360	δC42C45C48	364	δC8C5N1
		359	ρ'NC_3	360	ρ'NC_3
		341	δ_aNC_3 δ_aNC_3	344	δ_aNC_3
	337vw	335	δ_aNC_3	340	δC58C61C64, δC2C55C58
	288vw	278	δC11C14C17,δC20C23C26	291	τ_wCH_3(C77) τ_wN1-C5
	257vw	269	δC55C58C61	279	δC55C58C61
		248	δC36C39C42,τC30-C33	270	τ_wCH_3(C77)
		240	τ_wCH_3(C77)	246	δC42C45C48, δC36C39C42

229sh	228	τC61-C64	241	$\delta_a NC_3$
	225	$\tau_w CH_3$(C51), δC33C36C39	234	τ_wN1-C30
	223	$\tau_w CH_3$(C26)	225	$\tau_w CH_3$(C26)
	223	$\tau_w CH_3$(C51)	223	$\tau_w CH_3$(C51)
	213	$\tau_w CH_3$(C73)	217	$\tau_w CH_3$(C73)
208sh			205	τ_wN1-C5
	197	τC14-C17	199	τC14-C17
	195	τC58-C61,δC64C67C70	197	δC64C67C70
184sh	183	δC17C20C23	194	τ_wN1C30-H31
	172	τC33-C36	172	τ_wN1-C5
	158	τC5-C8	155	vH31-Cl81
			145	τC8-C11,δC30H31Cl81
139sh	137	τC39-C42	140	τC39-C42τC33-C36
128sh	132	τC45-C48	123	τC42-C45
121sh	118	τC42-C45	116	τC8-C11,$\tau_w NC_3$,τC55-C58
114sh	112	τC67-C70	114	τC67-C70
110sh	109	τC8-C11	110	τC5-C8,τ_wN1-C30
107sh	105	τC2-C55,τC30-C33	106	τC14-C17,τC5-C8
100sh	99	τC5-C8,τC30-C33	101	τC5-C8,τC11-C14
	95	τC5-C8,τC2-C55	99	τC5-C8
83vs	88	τC5-C8,τC8-C11	91	τC11-C14,τC5-C8
	78	τC11-C14,τC5-C8	79	τC45-C48,τC17-C20
72sh	74	τC20-C23	77	τC20-C23
72sh			67	δC30H31Cl81,vH31-Cl81
	62	τC30-C33	61	τC64-C67,τ_wC30-H31
	55	τC64-C67	56	τC11-C14,τC14-C17
	48	τC58-C61,$\tau_w NC_3$	52	τC61-C64
	45	τC36-C39	44	$\tau_w NC_3$,τ_wN1-C5
	40	τC17-C20	41	τC36-C39
			36	τC5-C8,τC8-C11
	30	τC58-C61,τC5-C8	33	τC5-C8
			24	τC5-C8,$\tau_w NC_3$
	18	$\tau_w NC_3$,τC2-C55	18	τC11-C14,τC14-C17
			12	τC30-C33
			10	τC2-C55,τC58-C61

Abbreviations: ν, stretching; wag, wagging; τ, torsion; ρ, rocking; τw, twisting; δ, deformation; a, antisymmetric; s, symmetric; [a]This work, [b]From Ref [15], [c]From scaled quantum mechanics force field with B3LYP/6-31G* method.

Table 2 shows clearly that in this region the positions and assignments of bands corresponding to CH_2 and CH_3 groups in the IL are different from the corresponding to cation due to effect of Cl anion that shift the bands at lower wavenumbers, as observed in the anti-symmetric CH_3 stretching modes ($\nu_a CH_3$(C77)). Besides, the anti-symmetric CH_2 mode of C30 atom linked to H31 in the IL is predicted at 2994 cm^{-1} while in the cation it mode is predicted at 2980 cm^{-1}. In this case in particular is notable the effect of Cl atom in the IL.

4.4.1.2. 1500-1000 cm^{-1} region. In this region, the effect of Cl also has influence on the positions of bands and assignments of IL, as compared with the cation. Thus, the SQM calculations predict the deformation, wagging and rocking modes of CH_2 groups and, the anti-symmetric and symmetric deformation and rocking modes of CH_3 groups for the cation different from those for the IL, as shown in Table 2. Here, in the 1508-1381 cm^{-1} region it is possible to observe coupling in the deformation modes of both groups. Therefore, the bands and shoulders observed in the IR and Raman spectra in that region are assigned to those deformation modes. The wagging modes of CH_2 groups for cation and IL are predicted from 1432 up to 1230 cm^{-1} while the rocking modes between 1423 and 1166 cm^{-1} and, for these reasons, these vibration modes can be assigned according to the SQM calculations and to assignments for species with similar groups [12,14,15]. In the cation, the rocking modes of CH_3 groups are predicted between 1188 and 1083 cm^{-1} while in the IL between 1195 and 1080 cm^{-1}. Also, in the cation, between 920 and 865 cm^{-1} are predicted other rocking modes while in the IL between 926 and 875 cm^{-1}. Consequently, the bands observed in both IR and Raman spectra in those regions are assigned to rocking modes. In addition in this region, C-C stretching modes and CCC and NC_3 deformation modes are predicted for both species by SQM calculations.

4.4.1.3. 1000-10 cm^{-1} region. For cation and IL, C-C, N-C stretching and twisting modes of CH_2 and CH_3 groups are expected in this region together with the H31···Cl81 stretching mode. In the cation, the N-CH_3 stretching mode is predicted at 958 cm^{-1} while in the IL at 949 cm^{-1} due to the presence of Cl anion. Hence, the weak Raman band at 959 cm^{-1} is assigned to that vibration mode of cation and to anti-symmetric N-C stretching mode of IL. The three N-C stretching modes considered with C_{3V} symmetries are predicted at 844, 801 and 758 cm^{-1} in the cation while in the IL at 850, 801 and 766 cm^{-1}. Note that the NC_3 deformation modes of cation and IL are predicted and assigned in practically the same regions. In cation and IL, the twisting CH_2 modes of different groups are predicted by SQM calculations in different regions while the three twisting CH_3 modes in both species are predicted in the same regions (234-213 cm^{-1}) although the $\tau_w CH_3$(C77) appear coupled with other modes in the IL, as detailed in Table 3. Here, the H31···Cl81 stretching mode is predicted by SQM calculations at 67 cm^{-1}, for which, it mode can be assigned to the shoulder observed in the Raman spectrum at 72 cm^{-1}.

4.5. Force Fields

In this work, the determination of harmonic force field of [Aliquat$^+$] [Cl$^-$] IL in the gas phase was computed with the SQMFF methodology and the Molvib program by using the B3LYP/6-31G* method while, for the cation it was taken of a previous work reported for the [Aliquat$^+$][NTf$_2^-$] IL in gas phase at the same level of theory [15]. Then, the scaled force constants for both species were calculated from their corresponding force fields and compared with reported for the [BMIM][OTF] IL and its cationic species in **Table 3** [12].

Table 3. Scaled internal force constants for [Aliquat$^+$][Cl$^-$] and its cation in gas phase compared with reported for [BMIM][OTF] by using the B3LYP method and different basis sets.

	B3LYP method			
Force constants	6-31G*[a]		6-311++G**	
	[Aliquat$^+$][Cl$^-$][a]	[Aliquat$^+$][b]	[BMIM][c]	[BMIM][OTF][c]
f(νN-CH$_3$)	3.86	3.95	4.40	5.06
f(νN-C$_3$)	2.45	3.49		
f(νCH$_2$)	4.73	4.75	4.73	4.73
f(νCH$_3$)	4.85	4.91	4.87	4.84
f(δCH$_2$)	0.81	0.79	0.77	1.28
f(δCH$_3$)	0.56	0.56	0.52	0.54

Units are mdyn Å^{-1} for stretching and mdyn Å rad^{-2} for angle deformations. [a]This work, [b]From Ref [15], [c]From Ref [12] for [BMIM][OTF].

Regarding first the force constants of [Aliquat$^+$] [Cl$^-$] IL and its cation, it is observed higher values in the *f(νN-CH$_3$)*, *f(νN-C$_3$)*, *f(νCH$_2$)* and *f(νCH$_3$)* force constants of cation, as compared with the corresponding to IL because the presence of Cl anion with higher electronegativity in the IL produces three new ionic H···Cl81 bonds decreasing the forces of other bonds, as was evidenced by NBO and AIM studies. Then, the effect of anion is higher in the quaternary N linked to the three side chains, as compared with the corresponding to N-CH$_3$ group. A very important observation is that despite of three larges side chains present in [Aliquat$^+$] and IL the values of *f(νCH$_2$)*, *f(νCH$_3$)*, *f(δCH$_2$)* and *f(δCH$_3$)* force constants are practically the same for both species and only slight differences are observed due to Cl in IL. When the values are compared with the [BMIM][OTF] IL and its cation we observed higher values in the *f(νN-CH$_3$)* force constant of these two species because the N atoms are linked to rings [12].

5. Conclusions

In this work, the [Aliquat$^+$][Cl$^-$] IL was structural and vibrationally characterized combining experimental FT-IR, FT-Raman and ^{1}H- and ^{13}C-NMR spectroscopies with theoretical studies based on hybrid B3LYP/6-31G* method. The theoretical structure of [Aliquat$^+$][Cl$^-$] IL determined in gas phase has shown tree ionic H···Cl bonds but only one of them with higher energy and lower distance between the involved atoms, as supported by atomic MK charges,

bond orders, NBO and AIM calculations. Hence, monodentate coordination between the [Aliquat$^+$] cation and Cl anion has been proposed to perform the vibrational assignments. The confirmation of optimized structure by NMR measurements has allowed the complete assignments of all bands observed in the infrared and Raman spectra with the aid of SQMFF methodology and the normal internal coordinates. The thermal stability shows that [Aliquat$^+$][Cl$^-$] start to decompose just above 200°C. The mapped MEP surface evidence a strong concentration of charges around the chloride anion compatible with nucleophilic sites in these regions while the frontier orbital analyses suggest that IL is most reactive than the cation probably due to the low values of both global electrophilicity and nucleophilicity indexes. Comparisons of gap values between [Aliquat$^+$][Cl$^-$] and [Aliquat$^+$][NTf_2^-] ILs show that the IL containing chloride is most reactive than the other one suggesting that the properties of an IL containing [Aliquat$^+$] are strongly dependent of anion. In addition, the scaled force constants for the [Aliquat$^+$][Cl$^-$] IL are reported while the comparisons with the corresponding to cation evidence the effect of Cl anion on its values.

Supplementary Information (SI).

Supplementary Information: **Tables S1-S3 and Figures S1-S3.**

ACKNOWLEDGEMENTS

This work was supported with grants from financial support by The Ministry of Higher Education and Scientific Research (MESRS) of Algeria in PRFU project code: B00L01UN200120180002 and, from CIUNT Project Nº 26/D608 (Consejo de Investigaciones, Universidad Nacional de Tucumán). The authors would like to thank Prof. Tom Sundius for his permission to use MOLVIB.

DECLARATION OF INTEREST STATEMENT

Mohammed Amin Assenine: Methodology; Data curation.

Boumediene Haddad: Conceptualization; Data curation; Supervision.

Annalisa Paolone: Conceptualization; Data curation.

Silvia Antonia Brandán: Validation; Visualization; Writing - original draft; Writing - review & editing.

Didier Villemin: Conceptualization; Project administration.

Mostefa Boumediene: Conceptualization; Data curation.

Mustapha Rahmouni: Conceptualization; Data curation.

Serge Bresson: Methodology; Resources.

CONFLICTS OF INTEREST

The authors declare no conflict of interest.

References

[1] M. Watanabe, M.L. Thomas, S. Zhang, K. Ueno, T. Yasuda, K. Dokko, Application of ionic liquids to energy storage and conversion materials and devices Chem. Rev.117 (2017) 7190- 7239.

[2] Y. Qiang, S. Zhang, L. Guo, X. Zheng, B. Xiang, S. Chen, Experimental and theoretical studies of four allylimidazolium-based ionic liquids as green inhibitors for copper corrosion in sulfuric acid, Corros. Sci. 119 (2017) 68-78.

[3] G.K. Dedzo, B.B. Nguelo, I.T. Kenfack, E. Ngameni, C. Detellier, Molecular control of the functional and spatial interlayer environment of kaolinite by the grafting of selected pyridinium ionic liquids, Appl. Clay Sci. 143 (2017) 445-451.

[4] B. Haddad, D. Mokhtar, M. Goussem, E.H. Belarbi, D. Villemin, S. Bresson, J. Kiefer, Influence of methyl and propyl groups on the vibrational spectra of two imidazolium ionic liquids and their non-ionic precursors, J. Mol. Struct. 1134 (2017) 582-590.

[5] B Haddad, J Kiefer, H Brahim, E H Belarbi, D Villemin, S Bresson, O Palumbo, Effects of C (2) methylation on thermal behavior and interionic interactions in imidazolium-based ionic liquids with highly symmetric anions, Applied Sciences 8 (2018) 1043-1061.

[6] L Ni, J Xin, K Jiang, L Chen, D Yan, X Lu, S Zhang, One-step conversion of biomass-derived furanics into aromatics by Brønsted acid ionic liquids at room temperature, ACS Sustain. Chem. Eng 6 (2018) 2541-2551.

[7] J Nawała, B Dawidziuk, D Dziedzic, D Gordon, S Popiel, Applications of ionic liquids in analytical chemistry with a particular emphasis on their use in solid-phase microextraction, Trac-Trend. Anal. Chem. 105 (2018) 18-36.

[8] Y Zhou, D Xu, L Zhang, Y Ma, X Ma, J Gao, Y Wang, Separation of thioglycolic acid from its aqueous solution by ionic liquids: Ionic liquids selection by the COSMO-SAC model and liquid-liquid phase equilibrium, J. Chem. Thermodyn. 118 (2018) 263-273.

[9] J. Kausteklis, V. Aleksa, M.A. Iramain, S.A. Brandán, Cation-anion interactions in 1-buthyl-3-methyl imidazolium nitrate ionic liquid and their effect on their structural and vibrational properties, J. Mol. Struct 1164 (2018) 1-14.https://doi.org/10.1016/j.molstruc.2018.03.100

[10] M Bystrzanowska, F Pena-Pereira, Ł Marcinkowski, M Tobiszewski, How green are ionic liquids?–A multicriteria decision analysis approach, Ecotoxicol. Environ. Saf. 174 (2019) 455-458.

[11] Y Pei, Q Lu, Y Niu, Y Zhao, Y Zhao, Z Li, J Wang, Aggregation Behavior of Pyrrolidinium Ionic Liquid Surfactants in− OH-Functionalized Ammonium-Based Protic Ionic Liquids, J. Chem. Eng. Data 64 (2019) 4708-4716.

[12] J. Kausteklis, V. Aleksa, M.A. Iramain, S.A. Brandán, DFT study and vibrational assignment of 1-Butyl-3-methylimidazolium trifluoromethanesulfonate ionic liquid by using the FT-Raman spectrum, J. Mol. Struct 1175 (2019) 663-676.

[13] S F G Gildeh, H Roohi, M Mehrdad, K Rad-Moghadam, K Ghauri, Experimental and theoretical probing of the physicochemical properties of ionic liquids composed of [Bn-DBU]+ cation and various anions J. Mol. Struct. 1202 (2020) 127226-127240.

[14] B Haddad, S A Brandán, A. M Amin, A Paolone, D Villemin, S. Bresson, Bidentate cation-anion coordination in the ionic liquid 1-ethyl-3-methylimidazolium hexafluorophosphate supported by vibrational spectra and NBO, AIM and SQMFF calculations, J. Mol. Struct. 128 (2020) 104-118.

[15] M.A. Assenine, B. Haddad, A. Paolone, S.A. Brandán, D. Villemin, M. Boumediene, M. Rahmouni, S. Bresson, Synthesis, thermal properties, vibrational spectra and computational studies of Trioctylmethylammonium bis (trifluoromethylsulfonyl) imide ionic liquid, Submitted to J. Mol. Struct. (2020).

[16] H Semghouni, S Bey, A Figoli, A Criscuoli, M Benamor, E Drioli, Chromium (VI) removal by Aliquat-336 in a novel multiframe flat sheet membrane contactor, Chem. Eng. Process 147 (2020) 107765.

[17] J P Mikkola, P Virtanen, R Sjöholm, Aliquat 336®—a versatile and affordable cation source for an entirely new family of hydrophobic ionic liquids, Green Chem. 8 (2006) 250-255.

[18] S K Panja, B Haddad, J Kiefer, Clusters of the Ionic Liquid 1-Hydroxyethyl-3-methylimidazolium Picrate: From Theoretical Prediction in the Gas Phase to Experimental Evidence in the Solid State, ChemPhysChem 19 (2018) 3061-3068.

[19] Y Liu, C Ma, S Men, Y Jin, An investigation of trioctylmethylammonium ionic liquids by X-ray photoelectron spectroscopy: The cation-anion interaction, J. Electron Spectrosc. 223 (2018) 79-83.

[20] M Mateescu, I C Bujanca, M Deaconu, The application of aliquat 336 as carrier in processes for wastewater treatment containing heavy metals, In Ecological and environmental chemistry 2017 (2017) 125-125.

[21] U Domańska, R Bogel-Łukasik, Physicochemical properties and solubility of alkyl-(2-hydroxyethyl)-dimethylammonium bromide, J. Phys. Chem. B109 (2005) 12124-12132.

[22] S Aparicio, M Atilhan, M Khraisheh, R Alcalde, Study on hydroxylammonium-based ionic liquids I. Characterization J. Phys. Chem. B115 (2011) 12473-12486.

[23] E Bodo, P Postorino, S Mangialardo, G Piacente, F Ramondo, F Bosi, R Caminiti, Structure of the molten salt methyl ammonium nitrate explored by experiments and theory, J. Phys. Chem. B115 (2011) 13149-13161.

[24] L F Faria, J R Matos, M C Ribeiro, Thermal analysis and Raman spectra of different phases of the ionic liquid butyltrimethylammoniumbis (trifluoromethylsulfonyl) imide, J. Chem. Phys. B116 (2012) 9238-9245.

[25] F M Vitucci, F Trequattrini, O Palumbo, J B Brubach, P Roy, M A Navarra, A Paolone, Stabilization of different conformers of bis (trifluoromethanesulfonyl) imide anion in ammonium-based ionic liquids at low temperatures, J. Phys. Chem. A118 (2014) 8758-8764.

[26] M S Miran, Yasuda T, M A B H Susan, K Dokko, M Watanabe, Binary protic ionic liquid mixtures as a proton conductor: high fuel cell reaction activity and facile proton transport, J. Phys. Chem. C118 (2014) 27631-27639.

[27] O Palumbo, F M Vitucci, F Trequattrini, A Paolone, A study of the conformers of the N, N-diethyl-N-methyl-N-propylammonium ion by means of infrared spectroscopy and DFT calculations, Vibrational Spectroscopy 80 (2015) 11-16.

[28] F Capitani, C Fasolato, S Mangialardo, S Signorelli, L Gontrani, P Postorino, Heterogeneity of propyl-ammonium nitrate solid phases obtained under high pressure, J. Phys. Chem. Solids 84 (2015) 13-16.

[29] Lima T A, Paschoal V H, Faria L F, Ribeiro M C, Giles C, Comparing two tetraalkylammonium ionic liquids. I. Liquid phase structure, J. Chem. Phys. 144 (2016) 224504-224513.

[30] B Haddad, A Paolone, D Villemin, M Taqiyeddine, E H Belarbi, S Bresson, J Kiefer, Synthesis, conductivity, and vibrational spectroscopy of tetraphenylphosphoniumbis (trifluoromethanesulfonyl) imide, J. Mol. Struct. 1146 (2017) 203-212.

[31] T Niemann, D Zaitsau, A Strate, A Villinger, R Ludwig, Cationic clustering influences the phase behaviour of ionic liquids, Sci. Rep. 8 (2018) 1-7.

[32] A.D. Becke, Density-functional exchange-energy approximation with correct asymptotic behavior, *Phys. Rev.* A38, 1988, 3098-3100.

[33] C. Lee, W. Yang, R.G. Parr, Development of the Colle-Salvetti correlation-energy formula into a functional of the electron density. *Phys. Rev.* B37, 1988, 785-789.

[34] P. Pulay, G. Fogarasi, G. Pongor, J.E. Boggs, A. Vargha, Combination of theoretical ab initio and experimental information to obtain reliable harmonic force constants. Scaled quantum mechanical (QM) force fields for glyoxal, acrolein, butadiene, formaldehyde, and ethylene. J. Am. Chem. Soc. 105 (1983) 7037-7047.

[35] G. Rauhut, P. Pulay, Transferable Scaling Factors for Density Functional Derived Vibrational Force Fields. *J. Phys. Chem.* 1995, 99, 3093-3100,

[36] T. Sundius, Scaling of ab-initio force fields by MOLVIB. *Vib. Spectrosc.* 2002, 29, 89-95.

[37] A.B. Nielsen, A.J. Holder, *GaussView*, User´s Reference, GAUSSIAN, Inc.: Pittsburgh, PA, USA, 2000-2003.

[38] Gaussian 09, Revision A.02, M. J. Frisch, G. W. Trucks, H. B. Schlegel, G. E. Scuseria, M. A. Robb, J. R. Cheeseman, G. Scalmani, V. Barone, B. Mennucci, G. A. Petersson, H. Nakatsuji, M. Caricato, X. Li, H. P. Hratchian, A. F. Izmaylov, J. Bloino, G. Zheng, J. L. Sonnenberg, M. Hada, M. Ehara, K. Toyota, R. Fukuda, J. Hasegawa, M. Ishida, T. Nakajima, Y. Honda, O. Kitao, H. Nakai, T. Vreven, J. A. Montgomery, Jr., J. E. Peralta, F. Ogliaro, M. Bearpark, J. J. Heyd, E. Brothers, K. N. Kudin, V. N. Staroverov, R. Kobayashi, J. Normand, K. Raghavachari, A. Rendell, J. C. Burant, S. S. Iyengar, J. Tomasi, M. Cossi, N. Rega, J. M. Millam, M. Klene, J. E. Knox, J. B. Cross, V. Bakken, C. Adamo, J. Jaramillo, R. Gomperts, R. E. Stratmann, O. Yazyev, A. J. Austin, R. Cammi, C. Pomelli, J. W. Ochterski, R. L. Martin, K. Morokuma, V. G. Zakrzewski, G. A. Voth, P. Salvador, J. J. Dannenberg, S. Dapprich, A. D. Daniels, Ö. Farkas, J. B. Foresman, J. V. Ortiz, J. Cioslowski, and D. J. Fox, Gaussian, Inc., *Wallingford CT*, 2009.

[39] E.D. Glendening, J.K. Badenhoop, A. D. Reed, J. E. Carpenter, F. Weinhold, NBO 3.1; Theoretical Chemistry Institute, *University of Wisconsin; Madison*, WI, 1996.

[40] R.F.W. Bader, Atoms in Molecules, A Quantum Theory, Oxford University Press, Oxford, 1990, ISBN: 0198558651.

[41] F. Biegler-Köning, J. Schönbohm, D. Bayles. AIM2000; A Program to Analyze and Visualize Atoms in Molecules, *J. Comput. Chem.* 2001, 22, 545.

[42] B.H. Besler, K.M. Merz Jr, P.A. Kollman, Atomic charges derived from semiempirical methods, *J. Comp. Chem.* 1990, 11, 431-439.

[43] G. Keresztury, S. Holly, G. Besenyei, J. Varga, A.Y. Wang, J.R. Durig. Vibrational spectra of monothiocarbamates-II. IR and Raman spectra, vibrational assignment, conformational analysis and *ab initio* calculations of *S*-methyl-*N*,*N*-dimethylthiocarbamate *Spectrochim. Acta*, 1993, 49A, 2007-2026.

[44] D. Michalska, R. Wysokinski, The prediction of Raman spectra of platinum(II) anticancer drugs by density functional theory, *Chemical Physics Letters*, 2005, 403, 211-217.

[45] R. Ditchfield, Self-consistent perturbation theory of diamagnetism. I. A gage-invariant LCAO (linear combination of atomic orbitals) method for NMR chemical shifts, *Mol Phys*. 1974, 27, 714–722.

[46] P. Ugliengo, MOLDRAW Program, University of Torino, Dipartimento Chimica IFM, *Torino, Italy*, 1998.

[47] J Haque, V Srivastava, C Verma, H Lgaz, R Salghi, M A Quraishi, N-Methyl-N, N, N-trioctylammonium chloride as a novel and green corrosion inhibitor for mild steel in an acid chloride medium: electrochemical, DFT and MD studies, New J. Chem. 41 (2017) 13647-13662.

[48] C Dong, X Song, E J Meijer, G Chen, Y Xu, J Yu, Mechanism studies on thermal dissociation of tri-n-octylamine hydrochloride with FTIR, TG, DSC and quantum chemical methods, J. Chem. Sci. 129 (2017) 1431-1440.

[49] M. Boumediene, B. Haddad, A. Paolone, M. Drai, D. Villemin, M. Rahmouni, S. Bresson, O. Abbas, Synthesis, thermal stability, vibrational spectra and conformational studies of novel dicationic meta-xylyl linked bis-1-methylimidazolium ionic liquids, J. Mol. Struct. 1186 (2019) 68-79.

[50] B. Haddad, A. Paolone, M. Drai, M. Boumediene, D. Villemin, E. H. Belarbi, & O. Abbas, Para-xylyl linked bis-imidazolium ionic liquids: A study of the conformers of the cation and of the anion-cation hydrogen bonding. J. Mol. Struct. 1175 (2019) 175-184.

Figure Captions

Scheme 1: Structure of investigated IL [Aliquat$^+$][Cl$^-$].

Figure 1. Hydrogen atom labeling and ^{1}H NMR (a), carbon atom labeling and ^{13}C NMR (b) in $CDCl_3$. of ([Aliquat$^+$][Cl$^-$]).

Figure 2. Optimized structures of [Aliquat$^+$][Cl$^-$] and its cation by using the B3LYP/6-31G* method.

Figure 3a. Orientation and direction of dipole moment vector corresponding to cation of [Aliquat$^+$][Cl$^-$] ionic liquid in gas phase by using the B3LYP/6-31G* level of theory.

Figure 3b. Orientation and direction of dipole moment vector of [Aliquat$^+$][Cl$^-$] ionic liquid in gas phase by using the B3LYP/6-31G* level of theory.

Figure 4. Coordination modes of Cl atoms to cation in the [Aliquat$^+$][Cl$^-$] IL.

Figure 5. Molecular graphic for the [Aliquat$^+$][Cl$^-$] IL in gas phase showing the geometry of all their bond critical points (BCPs), ring critical points (RCPs) and cage critical point (CCP) by using the B3LYP/6-31G* method.

Figure 6: TGA and DTA curves of ([Aliquat$^+$][Cl$^-$]) IL.

Figure 7. Experimental Infrared spectra of [Aliquat$^+$] [Cl$^-$] IL in solid phase compared with the predicted for the cation and IL in gas phase by using the hybrid B3LYP method.

Figure 8. Experimental Raman spectra of [Aliquat$^+$] [Cl$^-$] IL in solid phase compared with the predicted for the cation and IL in gas phase by using the hybrid B3LYP method.